Structural characterization of some sol–gel derived phosphosilicate glasses

ARTICLE *in* JOURNAL OF MOLECULAR STRUCTURE · APRIL 2015

Impact Factor: 1.6 · DOI: 10.1016/j.molstruc.2015.01.012

Journal of Molecular Structure 1086 (2015) 161–171

Contents lists available at ScienceDirect

Journal of Molecular Structure

journal homepage: www.elsevier.com/locate/molstruc

Structural characterization of some sol–gel derived phosphosilicate glasses

L. Todan [a], E.M. Anghel [a,*], P. Osiceanu [a], R.V.F. Turcu [b], I. Atkinson [a], S. Simon [b], M. Zaharescu [a]

[a] Romanian Academy, Institute of Physical Chemistry "Ilie Murgulescu", Spl. Independentei 202, 060021 Bucharest, Romania
[b] Babes-Bolyai University, Faculty of Physics & Interdisciplinary Research Institute on Bio-Nano-Sciences, 400084 Cluj-Napoca, Romania

HIGHLIGHTS

- Triethyl-phosphite/phosphate (TEP) and H_3PO_4 were P-sources to obtain $10P_2O_5$–$90SiO_2$.
- Spectral data by NMR, Raman, XPS and XRF was obtained for these gels and glasses.
- Un-hydrolyzed TEP in gel underwent partial vaporization and degradation by annealing.
- A 1.84 higher P_2O_5/SiO_2 ratio was found for the H_3PO_4 derived glass than TEP one.

GRAPHICAL ABSTRACT

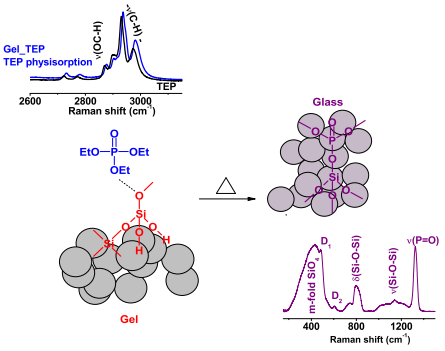

ARTICLE INFO

Article history:
Received 16 September 2014
Received in revised form 3 December 2014
Accepted 6 January 2015
Available online 23 January 2015

Keywords:
Phosphate glasses
Sol–gel method
Nuclear Magnetic Resonance (NMR)
Raman spectroscopy
Photoelectrospectroscopy (XPS)
X-ray fluorescence (XRF)

ABSTRACT

A comparative study of three phosphosilicate gels of the $90SiO_2$–$10P_2O_5$ composition obtained from tetraethoxysilane and three phosphorous precursors: triethylphosphate (TEP), triethylphosphite (TEPI) and H_3PO_4 is performed. ^{29}Si and ^{31}P Magic Angle Spining NMR, X-ray Photoelectron, X-ray Fluorescence and Raman spectroscopies as well as TG analysis are used in order to establish phosphorous precursors and annealing influence on composition and structure of the outcome materials. Unlike the three dimensional silicate network made of $Si(OSi)_x(OH)_{4-x}$ species, unreacted TEP (100% Q_1 condensed phosphorous units) from TEP derived gel and a large amount of isolated phosphorous species (39.7% Q_0) in the H_3PO_4 derived gel are identified. Annealing at 700 °C of the three gels give similar structure with the $90SiO_2$–$10P_2O_5$ glass, excepting the triethylphosphate derived glass that has a much lower P content. Thus, the H_3PO_4 derived glass at 700 and 1000 °C shows 1.89 and 1.94 times higher P_2O_5/SiO_2 ratios than in the case of the TEP derived one.

Introduction

Phosphate glass-containing materials have numerous technological uses (rare-earth ion hosts for solid-state lasers, planar waveguides, biomaterials, proton-conducting glass-based composite membranes for fuel cell, low-temperature sealing glasses etc.) due to their low melting temperature, high dimensional stability, ionic exchange and electrical conductivities [1–3].

Although, phosphosilicate glasses can be obtained by classical methods, their sol–gel synthesis offers the advantages of a lower cost process and advanced mixing of the starting materials up to molecular scale [4]. Various phosphorous precursors were employed along with tetraethoxysilane (TEOS) for sol–gel synthesis of the phosphosilicate gels. The mostly used phosphorous precursors in the sol–gel method were H_3PO_4, $OP(OC_2H_5)_3$ (TEP) and

* Corresponding author. Tel.: +40 21 316 79; fax: +40 21 312 11 47.
E-mail address: eanghel@hotmail.com (E.M. Anghel).

http://dx.doi.org/10.1016/j.molstruc.2015.01.012
0022-2860/

$P(OC_2H_5)_3$ or TEPI, although they presented some disadvantages. Different reactivity of the metal alkoxides towards hydrolysis and condensation was governed by electronegativity and coordination of the metal atom as well as steric factor of the alkoxide group [5]. Thus, Si- and P-alkoxides were found to react slowly in the sol–gel conditions [5,6]. Due to the lack of the TEP reactivity probed by ^{31}P NMR, Fernando-Lorenzo et al. [6] used H_3PO_4 as phosphorous source and the obtained materials by heat treatment of the gels at 300, 500 and 800 °C were highly non-homogeneous. Among the three phosphorous alkoxides used by Scrotter et al. [7], $OP(OC_2H_5)_3$ (TEP), $P(OC_2H_5)_3$ (TEPI) and $(OC_2H_5)_2$–O–$P(OC_2H_5)_2$, TEP was little reacted in sol after ten months while system with TEPI gave P—O—P and P—O—Si in the corresponding gel. Hydrolysis of TEOS was proven to be faster then the phosphorous alkoxides. Higher proton-conductive solid electrolyte was prepared from the TEOS and H_3PO_4 or TEP precursors [8]. Developing the water/vapor managed sol–gel processes [9] enabled faster obtaining of the high-proton conductive SiO_2–P_2O_5 electrolytes.

Despite the similar structure of silicates and phosphates consisting in corners sharing SiO_4 and PO_4, their solution chemistry depends on type and sensitivity of the alkoxides toward hydrolysis, i.e. type of the metallic atom and its ability to enhance the coordination number [10]. Extensive NMR investigations [4,10–13] of the phosphosilicate gels and corresponding glasses were carried out while Raman approach of their structure draws less attention [14,15]. Both Raman and NMR spectroscopies are versatile tools to monitor various stages of the whole sol–gel to glass preparation process [7,16,17]. Analogous to gels, the final glass structure is highly dependent on the synthesis parameters [18]. Thus, the four-coordinated silicon atoms (Q_n) in m-fold ring units [18] coexist with smaller amounts of six-coordinated silicon atoms in the gel-derived phosphosilicate glasses with 30 mol% P_2O_5 [11]. Instead, phosphorus atoms have always tetrahedral coordination in the phosphate glasses [19]. Connectivity and identification of the m-membered ring structure (where m represents the Q_n units forming a ring) of both silicate and phosphate glasses were considered according to the interconnected tetrahedral units, Q_n (where n stands for bridging oxygens, BOs, per tetrahedron unit) [14,19].

Our earlier studies concerning the sol–gel preparation of phosphosilicate gels underlined that type of the phosphorous reagents (TEP, TEPI and H_3PO_4) highly influences their composition and thermal behavior [20–24]. It is well known that H_3PO_4 reacts strongly with (TEOS) leading to the formation of Si—O—P bonds [20], while TEP does not hydrolyze or condense in the presence of TEOS [21]. In this way, the gelation in the latter system is assigned only to the TEOS whereas TEP is embedded in the Si—O—Si network [22–24]. The reaction mixture containing TEPI has an intermediate behavior due to its partial hydrolysis generating $HOP(OC_2H_5)_2$ [21] that could allow formation of hydrogen bonds between the OH of phosphorous compound and the OH of the silica network.

Hence, comparative structural investigations by Raman, NMR, XRF and XPS spectroscopies are carried out in this work to clear up stages of transformation of the liquid precursors (TEP, TEPI, H_3PO_4 and TEOS) into the resulted gels, as well as structural modifications underwent by these gels to glassy state as a result of the thermal treatment applied. Quantitative approach of the P_2O_5/SiO_2 ratio in the bulk of the obtained phosphosilicate glasses was attained from Raman and XRF spectroscopies.

Experimental procedure

Materials

Tetraethoxysilane, $Si(OC_2H_5)_4$ (TEOS) as silica precursor and three different types of phosphorous oxide precursors, namely: triethylphosphate $OP(OC_2H_5)_3$, triethylphosphite $P(OC_2H_5)_3$ and phosphoric acid, H_3PO_4 were used as starting materials in the sol–gel preparation. Ethanol was used as solvent, hydrochloric acid as catalyst and water for hydrolysis. The molar ratio of the reagents and preparation procedure of the phosphosilicate gels ($10P_2O_5$–$90SiO_2$), here named Gel_(TEP/TEPI/H_3PO_4), are presented in Table 1 as being selected based on the previous work [19]. Due to the high gelation tendency of the solution containing H_3PO_4 [23], its molar ratio of ethanol/precursors of silicon and phosphorous, i.e. Et(OH)/$\sum$precursors in Table 1, was raised to 10 instead of 4 as used for the other two solutions. Further, these gels were dried at room temperature, ground and thermally treated at: (a) 300 °C and 700 °C with 1 h plateau in both cases (named (TEP/TEPI/H_3PO_4)_700); and (b) at 1000 °C for an hour (called (TEP/TEPI/H_3PO_4)_1000).

Methods

Thermal analysis of the gels

The thermogravimetric analysis (TGA) was carried out by using a Mettler Toledo TGA/SDTA 851e equipment on ~25 mg of the Gel_(TEP/TEPI/H_3PO_4) samples in alumina crucibles, with a heating rate of 10 °C/min, in air, within 20–1000 °C temperature range.

Raman spectroscopy

The three gels and corresponding calcined samples at 700 and 1000 °C were analyzed by a LabRam HR spectrometer (Jobin–Yvon–Horiba) over 50–4050 cm^{-1} range. The 514 nm line of an Ar^+ laser at an incident power of 50 mW was used as exciting radiation through a 100 × objective of an Olympus microscope in a backscattering geometry and at a confocal hole of 200 μm. The spectral resolution was better than 2 cm^{-1}. A multipass cell holder was used to record Raman spectra of the TEOS, TEP and TEPI liquid precursors. The resulted spectra were background corrected and curves fitted by using the Igor 6.20 software.

NMR spectroscopy

The ^{31}P and ^{29}Si MAS NMR spectra of the as-prepared gels and phosphosilicate glasses thermally treated at 1000 °C were collected by using a Bruker AVANCE 400 spectrometer at a spinning frequency of 8 and 10 kHz for ^{29}Si and ^{31}P, respectively. The ^{29}Si and ^{31}P MAS NMR chemical shifts are expressed in ppm relative to 1% $Si(CH_3)_4/CDCl_3$ and H_3PO_4 water solution, respectively. All the spectra were processed using Bruker NMR programs and then they were deconvoluted using Dmfit program [25].

XPS measurements

Surface analysis performed by X-ray Photoelectron Spectroscopy (XPS) was carried out on a Quantera SXM equipment with a base pressure in the analysis chamber of 10^{-9} Torr. The X-ray source was Al Kα radiation (1486.6 eV, monochromatized) and overall energy resolution is estimated at 0.65 eV by the full width at half maximum (FWHM) of the $Au4f_{7/2}$ line. In order to take into account the charging effect on the measured Binding Energies (BEs) the spectra were calibrated using the C1s line (BE = 284.8 eV, C—C $(CH)_n$ bondings) of the adsorbed hydrocarbon on the sample surface. After recording the survey XPS spectra, the high resolution photoelectron spectra of the most prominent XPS transitions (C 1s, O 1s, Si2p and P2p) were collected for the Gel_(TEP/TEPI/H_3PO_4) and (TEP/TEPI/H_3PO_4)_700 samples. The estimated errors in quantification were hold in the range of ±10% for the relative concentrations and within ±0.2 eV for the Binding Energies (BEs) assignments.

Table 1
Experimental parameters for preparing gels in the binary mixture $90SiO_2$–$10P_2O_5$.

Gel	Precursor	Molar ratio			Reaction conditions		$pH_{mixture}$	$t_{gelling}$ (days)
		EtOH/Σ precursors	H_2O/Σ precursors	HCl/Σ precursors	T (°C)	t (h)		
Gel_TEP	TEOS, TEP	4	2	0.001	20	3	3.5	60
Gel_TEPI	TEOS, TEPI	4	2	0.001	20	3	3	30
Gel_H_3PO_4	TEOS, H_3PO_4	10	2	0.001	20	0.5	3	20

X-ray fluorescence (XRF) measurements

Elemental analysis of the samples was carried out using a wavelength dispersive X-ray fluorescence (WDXRF) spectroscopy method. The Rigaku ZSX Primus II spectrometer is equipped with an X-ray tube with Rh anode, 4.0 kW power, with front Be window, thickness: 30 μm. Set of 7 analyzing crystals (LiF200, LiF220, PET, Ge and 3 multi-layer crystals) facilitates qualitative and quantitative analysis of elements ranging from beryllium (Be) through uranium (U). The XRF data were analyzed using EZ-scan combined with Rigaku's SQX fundamental parameters software (standard less) which is capable of automatically correcting all matrix effects, including line overlaps.

Results

In the experimental conditions mentioned above and for all phosphorous-precursors used, homogeneous and transparent gels were obtained. The influence of the precursor on their thermal behavior was first studied by TG/DTA analysis (DTA curves presented elsewhere [22]). Moreover, thermal analysis was carried out in air to simulate the conditions in which these materials are used (in fuel cells, for example).

Thermal analysis of the gels

The mass losses (TG) of the three gels are presented in Fig. 1 and Table 2 in accordance with the data previously reported [20,22]. Thus, bellow 150 °C, water and solvent were eliminated from all three samples, leading to a weight drop on all TG curves (Fig. 1, Table 2).

During the next temperature range, 150–400 °C, the evolution or decomposition of the organic and residues took place. Moreover, OH evolution was not ruled out in the same temperature range.

Among the three gels, the largest mass loss of ~20% was observed for the Gel_TEP pointing out its highest organic content. Above 400 °C, structural OH evolution caused very slight mass changes, in all three gels. The results are in good agreement with the previously reported ones [22].

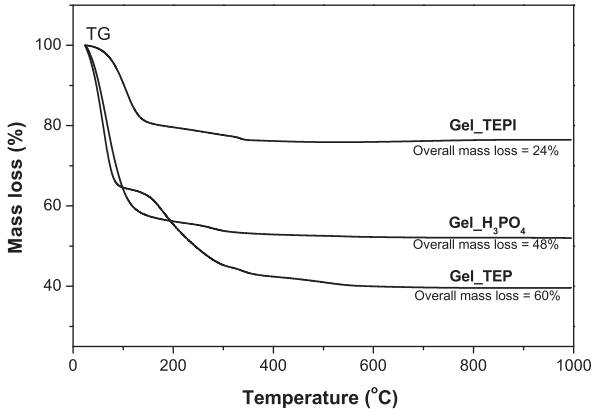

Fig. 1. TG curves of the phosphosilicate gels: Gel_(H_3PO_4/TEPI/TEP).

Raman spectroscopy

Raman spectra of the phosphosilicate gels under discussion are illustrated in Fig. 2 while the deconvolution results in the 60–2000 cm^{-1} domain and band assignments were listed in Table 3.

Since phosphorous precursors and heat treatment of the obtained gels are two important parameters in obtaining the phosphosilicate glasses, Fig. 3 illustrates Raman spectra of the Gel_(TEP/TEPI/H_3PO_4), (TEP/TEPI/H_3PO_4)_(700/1000) samples and the liquid precursors: TEOS, TEPI and TEP within 60–2000 cm^{-1} domain. Analog to the Raman spectra of SiO_2 and P_2O_5–SiO_2 materials [33], the Raman spectra of the Gel_(TEP/TEPI/H_3PO_4), (TEP/TEPI/H_3PO_4)_700 samples in Fig. 3 can be divided in two regions, i.e. <700 cm^{-1} and 700–2000 cm^{-1}. In the case of the (TEP/TEPI/H_3PO_4)_1000 glasses, the two regions are narrower (bellow 650 cm^{-1} and 650–1400 cm^{-1}, respectively). A *third region*, above 2300 cm^{-1}, should be considered in order to obtain information about hydrogen bonding in the partially reacted phosphorous precursors and hydrolyzed species present in gels.

The *first region* bellow 700 cm^{-1} gives information on the silicate network formation in gels [26] and type of the *m*-membered rings of the interconnected tetrahedral units, Q_n (*n* stands for the bridging oxygen atoms), of the silicate glassy network [34,35]. Deconvolution of this region for the TEP_(700/1000) samples is illustrated in Fig. 4. The first three deconvoluted bands (Fig. 4b for the TEP_1000 glass and Table 4 for the (TEP/TEPI/H_3PO_4)_1000 glasses) originate from the 5–7-membered rings of the condensed silica units while the next bands at 492 cm^{-1} (FWHM ~30 cm^{-1}) and 606 cm^{-1} are due to the 4- and 3-membered ring defects, respectively. Conversely, due to the irregular structure of the silicate gels, neither ring defect bands, i.e. bands located at 490 and 607 cm^{-1}, nor Si—O—Si network bands at 1180 and 1070 cm^{-1} [27,28] are noticeable in Fig. 3 for the Gel_(TEP/TEPI/H_3PO_4). The band at about 480 cm^{-1} (Table 3) of the Raman spectra of the three gels under discussion originates from $Si(OSi)_3(OR)$ [28] (where *R* stands for C_2H_5 or H). The strong band at 430 cm^{-1} band of the Gel_H_3PO_4 (Fig. 3c) is attributable to $Si(OSi)_4$. The Si—O—C modes of TEOS at ~649 cm^{-1} are barely visible in Fig. 3 for the three gels. Narrower bands are recorded for the (TEPI/H_3PO_4)_700 samples in the first region as a consequence of the particle coalescence during the intermediate stage of the gel-to-glass transformation in the silicate systems [28]. The first stage of transformation above 350 °C is considered to be formation of the threefold planar ring (607 cm^{-1} band) while the third one (above 800–1100 °C) consists in modification of the internal structure and glass relaxation and thus their Raman spectra resemble the ones of the conventional melt quenching glasses.

Vibration modes in the *second region* 700–2000 cm^{-1} range for gels and 650–1450 cm^{-1} for glasses), proves the reactivity of the phosphorous precursors and presence of the P—O—Si bonds (1140 cm^{-1}). The P_2O_5 content in a phosphosilicate glass is proportional with the intensity ratio: I_{1325}/I_{800}, these bands originating from the P═O and the Si—O—Si vibration modes. Since the width of the Raman bands at 800 and 1325 cm^{-1} varies within the (TEP/TEPI/H_3PO_4) glasses areas of the two bands were considered instead of their intensities (see Table 4). Also, symmetric and asymmetric bending modes of the —CH_2 and —CH_3 groups of the

Table 2
Mass loss obtained from the thermo gravimetric analysis of the Gel_(TEP/TEPI/H_3PO_4) samples, in air.

ΔT (°C)	Δm (%)			Assignments
	Gel_TEP	Gel_TEPI	Gel_H_3PO_4	
25–150	37.4747	19.0034	42.4772	Elimination of adsorbed H_2O and ethanol
150–400	20.0933	4.9935	4.6317	Organic decomposition and combustion, structural OH elimination
400–1000	2.8067	0.2826	0.8906	Structural OH elimination
Total mass loss (%)	60.3747	24.2795	47.9995	

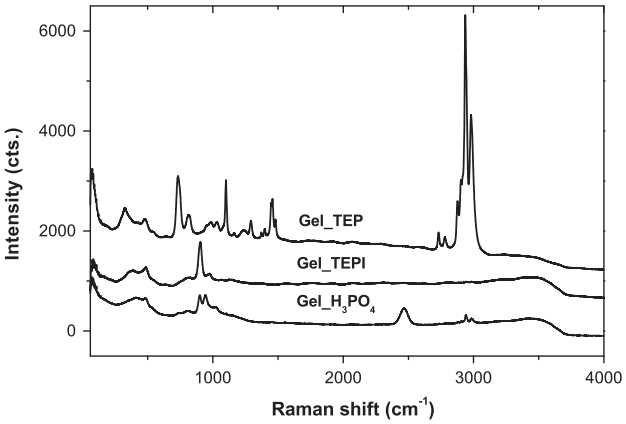

Fig. 2. Raw Raman spectra of the TEOS gels with: TEP, TEPI and H_3PO_4 precursors.

partially reacted TEOS and phosphorous alkoxides were included in the *second region*, i.e. over 1340–1650 cm^{-1} domain, for the obtained gels. All the Raman modes of the unreacted TEP (i.e. 733, 813, 1032 and 1098, 1162, and 1279 cm^{-1} corresponding to the PO_3 symmetric stretch, PO_3 asymmetric stretch, C—O stretch, CH_3 rocking, and P═O symmetric stretch [30]) are identified in this region for the Gel_TEP (Fig. 3a) while its 1279 cm^{-1} mode splits into 1241 and 1292 cm^{-1} modes. Stretching vibration of the $\nu_s\{P(OH)_3\}$ in the aqua solution of the H_3PO_4 [31] is shifted to 899 cm^{-1} in the case of the Gel_H_3PO_4 (Fig. 3c). Formation of the graphitic materials in the (TEP/TEPI/H_3PO_4)_700 samples is evidenced by the D and G bands [35] located within 1200–1650 cm^{-1} in Fig. 3.

Given the fact that TEOS and two phosphorous alkoxide, TEPI and TEP, were used to prepare the Gel_(TEP/TEPI) materials, the high frequency Raman spectra included in *the third region* of the TEOS, TEP and Gel_TEP are illustrated in Fig. 5. Moreover, the IR assigned band at ~2497 cm^{-1} to the ν(O═P—OH) [9] was located at 2469 cm^{-1} in the Raman spectrum of the Gel_H_3PO_4 sample (Fig. 2) as a measure of the partially unreacted H_3PO_4. The very strong bands within 2685–3140 cm^{-1} for the Gel_TEP in Figs. 2 and 5 correspond to the stretching vibrations of the OC—H, C—H bonds in TEP (2869, 2926 and 2973 cm^{-1}) and not to the TEOS component with different symmetric stretching modes CH_2 and CH_3 groups. Whereas the C—H stretch modes of the Gel_TEPI and Gel_H_3PO_4 materials almost vanishes (Fig. 2), the next region up to 3910 cm^{-1}, originating from the O—H vibrations [15,32] in waters and silanols groups, enhances. The weak band at 2880 cm^{-1} of the Gel_H_3PO_4 (Fig. 2) originates from the small amount of the residual TEOS. The weak shoulder at 3811 cm^{-1} of

Table 3
Deconvolution results (peak position and width) of the Raman spectra within 100–2000 cm^{-1} range for the Gel_(TEPI/H_3PO_4/TEP) gels and the band assignments.

Gel_TEPI	Gel_H_3PO_4	Gel_TEP	Assignment	References
161/100	139/96	122/111	Skeletal siloxane	[26]
	332/74	324/63	δ(O—P—O) in PO_4 tetrahedra	[19]
		368/23	δ(O—P—O) in TEP	
394/131				
	432/156	430/164	Silane network bending, ν_2 (E_1/A) in PO_4^{3-} (432 cm^{-1})	[27,28]
485/56	487/30	482/34	Tetraxiloxane rings	[26–28]
549/48	539/49	544/25		
644/750	647/59	645/37	Si—O—C vibrations	[27,28]
	739/58	736/37	Symmetric stretching vibration of P—O—(C) (726 cm^{-1}) and PO_3 symmetric stretch (733 cm^{-1})	[29,30]
794/109	805/67	812/47	Si—O—Si symmetric stretch (804 cm^{-1}), PO_3 asymmetric stretch (813 cm^{-1}) and CH_2-rocking (810 cm^{-1})	[14,26,30]
902/30	899/25		P—O stretching mode of the H_3PO_4 (890 cm^{-1})	[31,15]
		919/44	δ(Si—OH) (912 cm^{-1}) and $\delta(CH_2)$	[15,26]
937/175	942/30	952	ν_s(C—C) of fully ethoxide terminated monomers (933 cm^{-1}), δ(Si—OH) (929 cm^{-1}) and $\nu_a\{P(OH)\}$ (942 cm^{-1})	[26,15,31]
974/28	964/181	980/72	ν_1 of PO_4^{3-} (962 cm^{-1})	[11]
1067/57	1024/27		ν_a(Si—O) of loci with 3- and 4-fold rings (1000–1200 cm^{-1})	[14]
		1034/30	ν(C—O) in TEP (1032 cm^{-1})	[30]
1140/100	1150/176	1093/30;	ν_a(Si—O) of loci with 3- and 4-fold rings (1000–1200 cm^{-1}), ν_a(P—O) (1087 cm^{-1}), δ(Si—OH)	[14,19,30]
		1101/12	ν(C—O) at 1098 cm^{-1} in TEP	[30]
		1166	CH_3 rocking in TEP (1162 cm^{-1})	[30]
1236/86		1241/49	$\nu_a(PO_4)$ of Q_2 units	[19]
		1292/21	P═O symmetric stretch in TEP (1279 cm^{-1})	[30]
1379/108	1397/26	1372/8	$\delta_s(CH_3)$	[26]
		1397/13	Wagging of CH_2 group (1398 cm^{-1})	
		1447/11		
	1454/27	1459/47	$\delta_a(CH_3)$	[26]
		1482/8	$\delta_a(CH_2)$	
1563/99	1548/79			
	1610/61		Vibration modes of OH units	[32]
1756/125	1747/179	1776/124	δ (H—O—H)	[15]
1922/78	1926/90	1915/77	ω (H—O—H) and vibration of external H_2O molecules)	[15,32]

NBO stands for non-bridging oxygen.

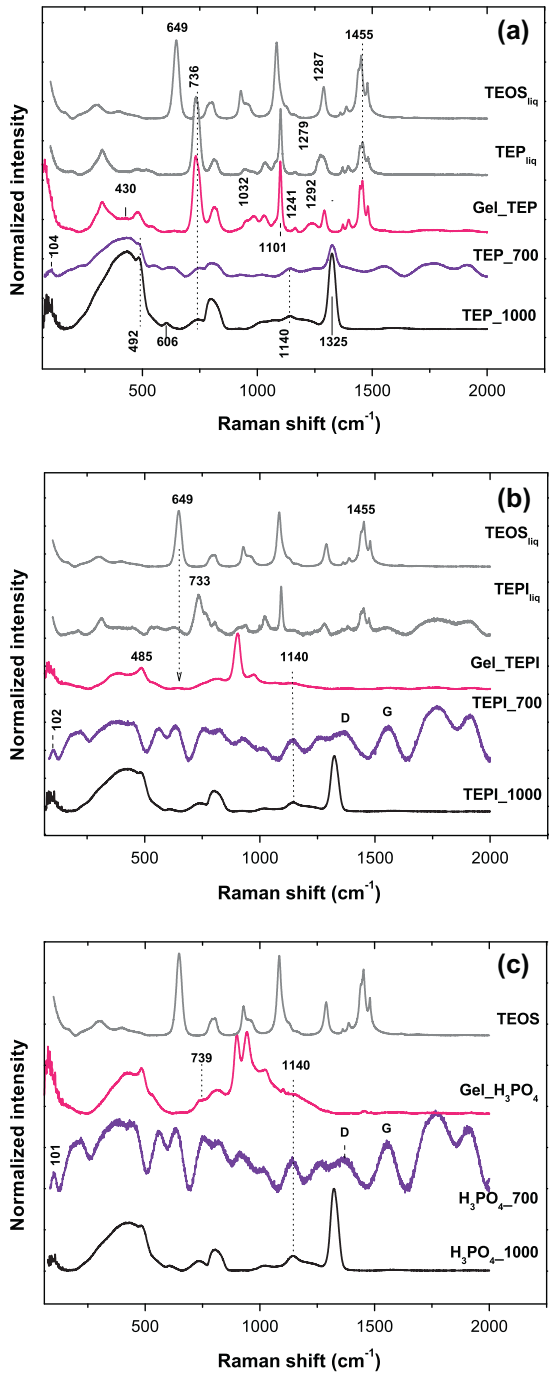

Fig. 3. Raman spectra of the TEOS with (a) TEP-, (b) TEPI- and (c) H_3PO_4-containing materials within 65–2000 cm^{-1} spectral range.

the Gel_TEP in Fig. 2 is ascribed to the SiO—H stretching vibrations in non-hydrogen-bonded silanols (isolated groups) analog to the sol–gel silicate glasses at 3750 cm^{-1} as reported by Aguiar et al. [14,36].

MAS NMR spectroscopy

The recorded ^{29}Si MAS NMR spectra of thus prepared gels and heat treated samples at 1000 °C are presented in Figs. 6 and 7, respectively.

In silicates, the four oxygen atoms of a [SiO_4] structural unit can be bound or not forward to other silicon atoms, being nominated as bridging (BO) and non-bridging oxygen (NBO), respectively.

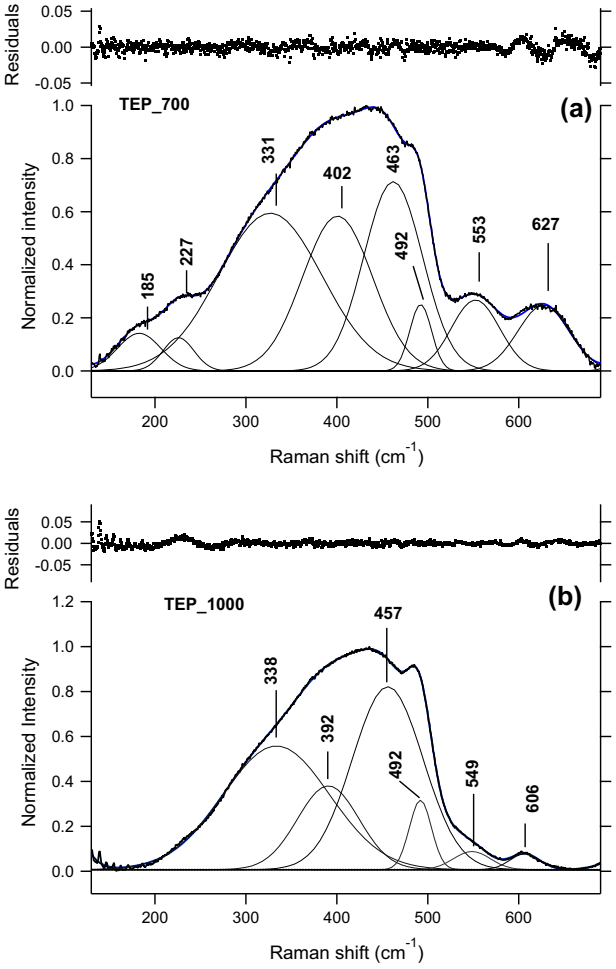

Fig. 4. Deconvolution of the Raman spectra of the TEP derived glasses at: (a) 700 °C and (b) 1000 °C within 130–690 cm^{-1} domain.

Each of these possible [SiO_4] units having none, one, two, three or four bridging oxygens interconnecting two [SiO_4] tetrahedra, are noted using Q_n terminology (n is the number of BOs), that is the main approach in silicon units characterization [37–39]. The chemical shift mean values for these units are between −70 ppm for Q_0 and −120 ppm for Q_4 units [37].

The recorded ^{31}P MAS NMR spectra of thus prepared gels are presented in Fig. 8 and for samples obtained at 1000 °C in Fig. 9. Structural network in the phosphate systems can be described using the same Q_N terminology, where N is the number of BOs per P atom. Unlike silicon, which can occur in five different units, the [PO_4] tetrahedra present a double bounding P═O, so only four phosphorus units can exist in oxide systems [40,41].

In the case of phosphosilicates there is the possibility to have interconnected [SiO_4] units with [PO_4] units named: $Si(OSi)_n(OX)_{4-n}$ and $OP(OP)_N(OX)_{3-N}$ units [41,42]. It is generally accepted that such connections have contributions on the NMR lines corresponding to different Q_n units at the higher chemical shift values. Particularly for the lines corresponding to the Q_3 units in ^{31}P MAS NMR spectrum or to the Q_4 units in the ^{29}Si MAS NMR spectrum, will have a shoulder on that side [41,42].

Having in view all these assignments we deconvoluted the recorded MAS NMR spectra by using the Dmfit program [25]. The results of these deconvolutions are presented in Table 5, for ^{29}Si MAS NMR spectra, and in Table 6, for ^{31}P MAS NMR spectra.

Table 4
Gaussian deconvolution results of the Raman spectra (150–1450 cm^{-1}) of the (TEP/TEPI/H_3PO_4_1000) glasses and band assignments.

TEP_1000 Peak/FWHM (cm^{-1})	TEPI_1000 Peak/FWHM (cm^{-1})	H_3PO_4_1000 Peak/FWHM (cm^{-1})	Assignment	References
343/142	340/139	327/128	7-, 6-, 5-membered rings of SiO_4	[34]
389/74	390/77	393/91		
455/95	458/106	463/106		
492/28	492/30	493/33	4-membered ring defect	[18]
549/42	553/37	553/45		
6067/38	613/53	611/51	3-membered ring defect	[18]
727/52	729/60	729/57	ν_s(P—O—P) in PO_4 tetrahedra	[19]
806/62	808/62	809/57	Symmetric stretch motion of BOs in silicate network	[34]
–	920/44	910/37	Si—O—NBO stretching at 900–970 cm^{-1}, ν_s $(PO_4)^{3-}$	[14,19]
1012/47	1016/55	1036/104	ν_a(Si—O) of loci with 3- and 4-fold rings (1000–1200 cm^{-1})	[14]
1062/57	–	–	Split of the 806 cm^{-1} mode	[34]
1140/38	1144/45	1141/62	$\nu_a(PO_3^{2-})$ in Q_1 units and $\nu_a(PO_4)^-$ in Q_2 units	[17]
1166/239	1186/232	1215/108	Split of the 806/808 and 809 cm^{-1} modes	[34]
1325/35	1325/37	1325/39	ν(P=O) in P_2O_5 network	[33]
1.33	1.55	2.58	A_{1325}/A_{806}	

BO stands for bridging oxygen atoms.

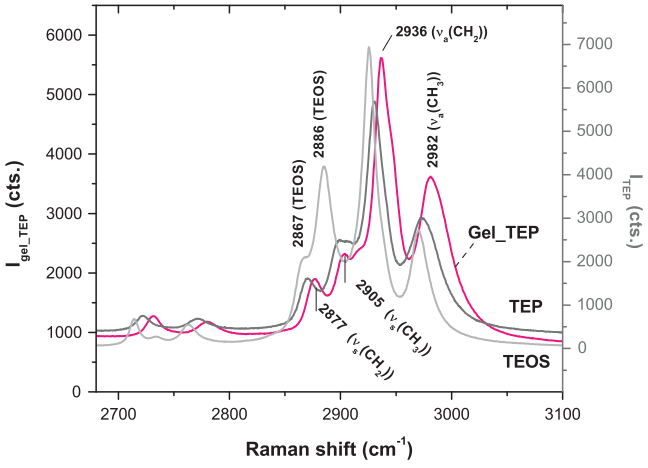

Fig. 5. Comparative C—H stretching bands of the TEOS, TEP and Gel_TEP.

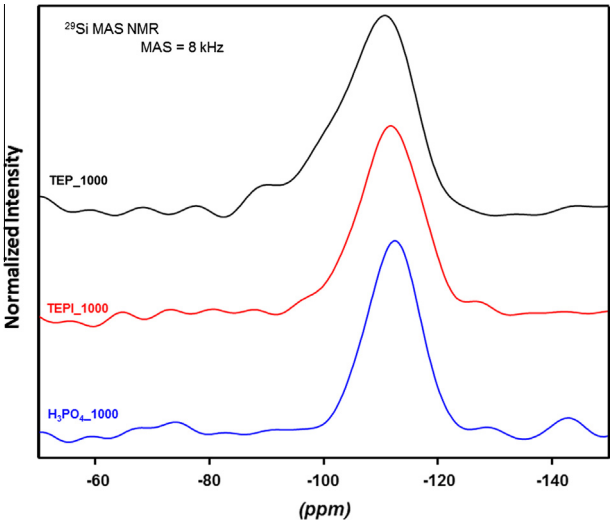

Fig. 7. ^{29}Si MAS NMR spectra of the (H_3PO_4/TEPI/TEP)_1000 glasses.

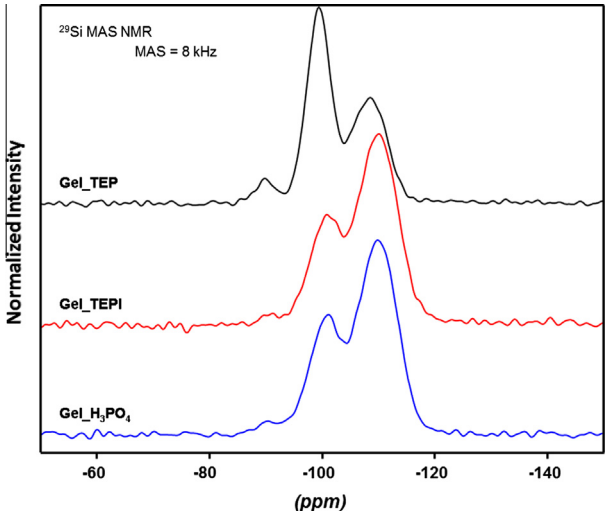

Fig. 6. ^{29}Si MAS NMR spectra of the Gel_(H_3PO_4/TEPI/TEP) samples.

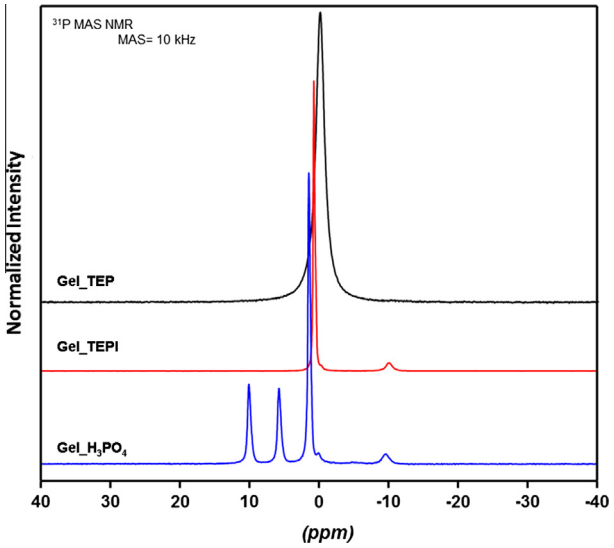

Fig. 8. ^{31}P MAS NMR spectra of the Gel_(H_3PO_4/TEPI/TEP) samples.

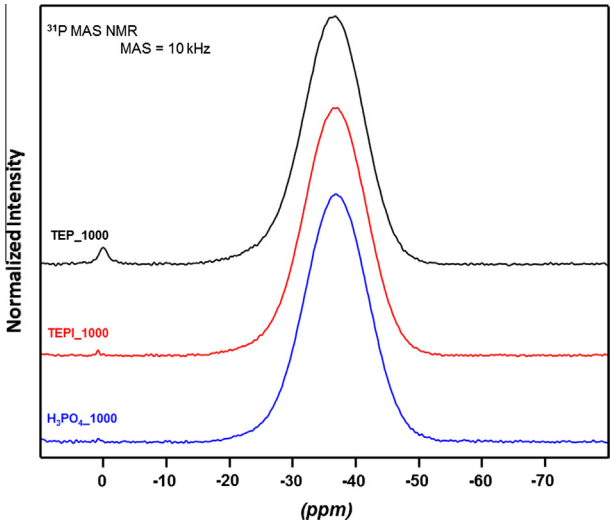

Fig. 9. ^{31}P MAS NMR spectra of the (H_3PO_4/TEPI/TEP)_1000 glasses.

Table 5
^{29}Si MAS-NMR peak positions and full width half maximum (FWHM) for the Gel_(TEP/TEPI/H_3PO_4) and the corresponding glasses (TEP/TEPI/H_3PO_4)_1000.

Sample	Q_n*	δ(^{29}Si) (ppm)	^{29}Si FWHM (ppm)	Intensity (%)
Gel_TEP	Q_2	−90.50	4.69	5.5
	Q_3	−99.83	5.10	52.3
	Q_4	−108.81	7.38	42.2
Gel_TEPI	Q_2	−90.99	4.60	2.1
	Q_3	−100.55	6.75	33.2
	Q_4	−109.95	8.15	64.7
Gel_H_3PO_4	Q_2	−91.25	6.67	3.3
	Q_3	−100.49	6.61	31.3
	Q_4	−109.91	7.94	65.4
TEP_1000	Q_3	−99.46	10.13	29.2
	Q_4^1	−110.75	10.20	58.3
	Q_4^2	−114.10	9.80	12.5
TEPI_1000	Q_3	−100.18	9.35	11
	Q_4^1	−110.70	9.73	66.2
	Q_4^2	−114.50	9.44	22.8
H_3PO_4_1000	Q_4^1	−110.90	10.17	68.2
	Q_4^2	−114.70	9.18	31.8

* Q_n stands for tetrahedral Si sites with n bridging oxygen atoms.

XPS and XRF data

The XPS analysis was used to determine the oxidation states of the elements present on the surface and, after quantitative analysis, to find the element and oxidation state relative concentrations, as well. The XPS data were summarized in Figs. 10 and 11 as well as in the Table 7 for the Gel_(H_3PO_4/TEPI/TEP) materials and Table 8 for the thermally treated gels (H_3PO_4/TEPI/TEP)_700 glasses. The C 1s data of the gels in Table 7 shows the presence of the carbon from various oxygenated carbons [43] of the unreacted alkoxides, hydrolysis and condensation compounds and traces of CO_2 (binding energies, BE, within 285–290 eV), as well as hydrocarbon (BE of 284.8 eV) adsorbed on the outermost surface layer.

The Si/P atomic ratios of the (TEP/TEPI/H_3PO_4)_700 samples were summarized in Table 8. Various Si/P ratios derived from XRF and XPS data were consisted in the different scale of examination for the two techniques, i.e. nanometer scale in case of the XPS [23]. Smaller Si/P ratio derived by XPS measurements than the one from the XRF of the (TEPI/H_3PO_4)_700 samples might be consistent with the more abundant phosphorous content on the surface [44].

Table 6
^{31}P MAS-NMR peak positions and full width half maximum (FWHM) for the Gel_(TEP/TEPI/H_3PO_4) and the corresponding glasses (TEP/TEPI/H_3PO_4)_1000.

Sample	Q_N[a]	δ(^{31}P) (ppm)	^{31}P FWHM	Intensity (%)
Gel_TEP	Q_1	−0.01	1.48	100
Gel_TEPI	Q_1^1	0.91	0.24	69.8
	Q_1^2	0.68	0.68	19.9
	Q_1^3	−0.19	0.24	0.9
	Q_2	−9.92	1.07	9.4
Gel_H_3PO_4	Q_0^1	9.98	0.56	20.1
	Q_0^2	5.66	0.58	19.6
	Q_1^1	1.42	0.30	32.8
	Q_1^2	1.23	0.45	17.8
	Q_1^3	0.05	0.48	2.2
	Q_2	−9.64	1.37	7.5
TEP_1000	Q_1	−0.05	1.89	1.2
	Q_3^1	−35.0	9.29	59.0
	Q_3^2	−39.0	9.13	39.8
TEPI_1000	Q_3^1	−35.0	10.58	44.8
	Q_3^2	−38.2	11.68	55.2
H_3PO_4_1000	Q_3^1	−35.0	11.60	31.5
	Q_3^2	−39.0	11.30	68.5

[a] Q_N stands for tetrahedral P sites with N bridging oxygen atoms.

If the Si/P ratio, ratio obtained from the XRF data, of 4.63 for the TEPI_700 was close to the ones for H_3PO_4_700 (3.97) and theoretically predicted $90SiO_2$–$10P_2O_5$ (3.80), much phosphorus depleted TEP_700 was found according to its Si/P ratio of 7.50 obtained from the XRF data.

Discussions

Phosphorous precursor influence on the structure of gels

Different mass losses on heating of the Gel_(TEP/TEPI/H_3PO_4) sample in Fig. 1 are clearly dependent on the type of the phosphorous precursor used and implicitly on the phosphorous compounds formed during preparation of the three gels.

According to the Raman findings of the *first region* within 150–700 cm^{-1} (Figs. 2 and 3) for all Gel_(TEP/TEPI/H_3PO_4) samples, the TEOS precursor underwent both hydrolysis (almost vanishing of the 643–653 cm^{-1} band assignable to the four groups (—OC_2H_5) attached to the atom of silicon):

$$Si(OC_2H_5)_4 + xH_2O \rightarrow (C_2H_5O)_{4-x}Si(OH)_x + xC_2H_5OH \quad (1)$$

and condensation:

$$(C_2H_5O)_{4-x}Si(OH)_x + (OH)_ySi(C_2H_5O)_{4-y} \rightarrow (C_2H_5O)_{4-x}(OH)_{x-1}$$
$$Si-O-Si(OH)_{y-1}(C_2H_5O)_{4-y} + H_2O \rightarrow SiO_2 \quad (2)$$

when the Raman bands at 432 and 487 cm^{-1} pointed out to formation of silane or siloxane [26]. In fact, intensity of the 645–653 cm^{-1} band is a measure of the hydrolysis efficiency [16,27,28]. Almost vanishing of the Raman bands of the —CH_2 and —CH_3 over 1340–1650 cm^{-1} and highly decrease of the 1085 cm^{-1} band attributable to Si—O—C (Fig. 3 and Table 3) point out hydrolysis and condensation completion of the TEOS and formation of the $Si(OSi)_3(OR)$ and $Si(OSi)_4$ with the strongest bands at 487 and 432 cm^{-1} for the Gel_H_3PO_4 in comparison to the other two gels. This is in accordance with NMR data in Table 5 where less interconnected network is found for the TEP based gel (42.2% Q_4) while for Gel_TEPI and Gel_H_3PO_4 64.7% and 65.4% Q_4 species are recorded. Although, three dimensional silicate network, consisting of Q_2, Q_3 and Q_4 condensed silicon units, i.e. $Si(OSi)_x(OH)_{4-x}$ species (where x was within 1–4), are depicted for the three gels under discussion (see Table 5),

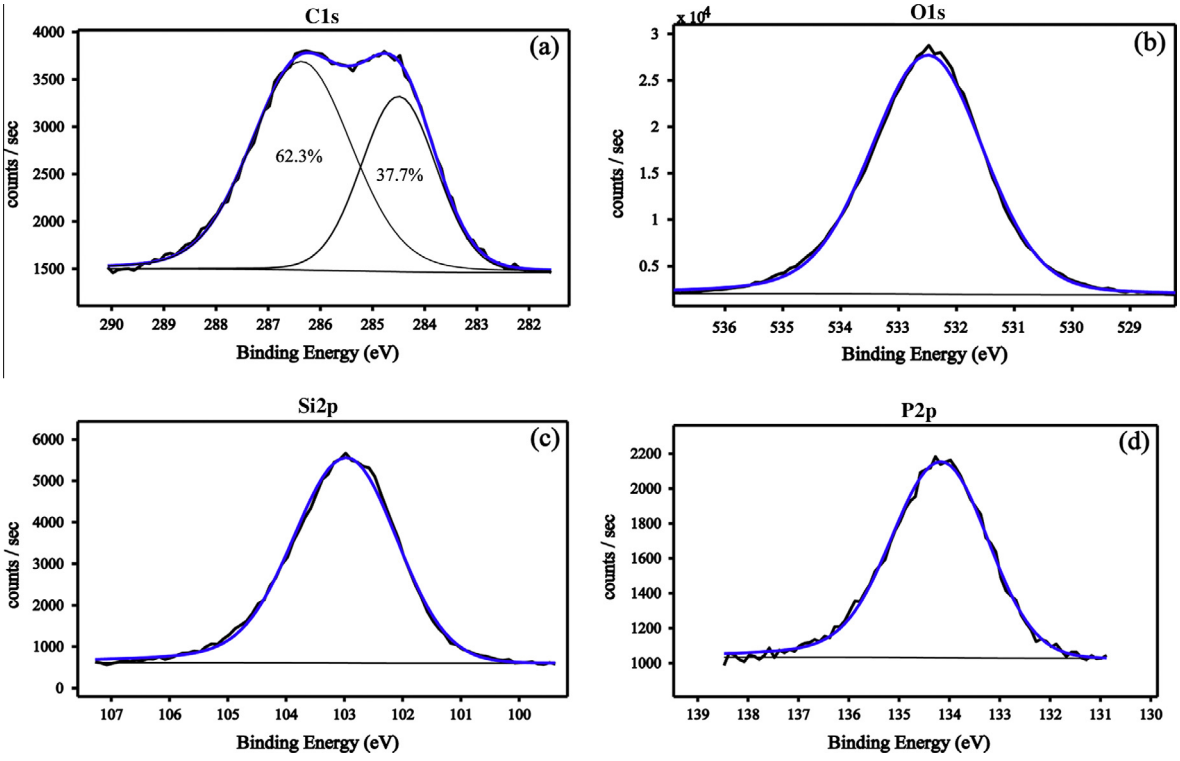

Fig. 10. Deconvoluted XPS spectra of the Gel_TEP: (a) C1s, (b) O1s, (c) Si2p, and (d) P2p.

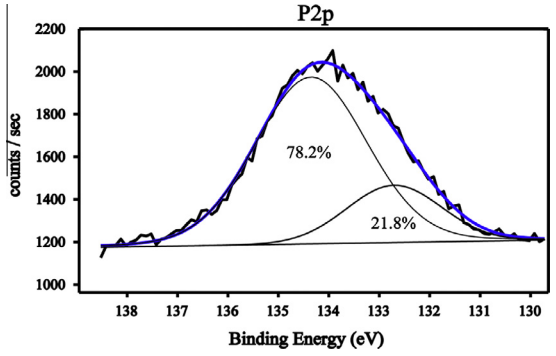

Fig. 11. The P 2p XPS deconvoluted spectrum for the TEP_700 sample.

however presence of the $Si(OSi)(OH)_2(OP)$ at about −100 ppm and $Si(OSi)_2(OP)(OH)$ at about −109 ppm can not be ruled out for the Gel_($TEPI/H_3PO_4$) [12]. The single peak of the O1s spectrum (Fig. 10b) exhibits that the most prominent amount of oxygen bounded into the sample lattice as O^{2-} while the Si spectral signature revealed the full oxidation state 4+ as SiO_2 [45] (Fig. 10c).

The most pronounced difference between the local structures of these gels is observed around phosphorus. Taking the advantage of the Raman investigations of the phosphorous liquid precursors enables us to identify Raman modes within *second region* of the Raman spectra of the unreacted TEP component in the Gel_TEP sample (Figs. 2, 3a, and 5). Hence, one can consider that ^{31}P MAS NMR line in Fig. 8 and Table 6 was coming from isolated and immobilized TEP rich areas. The unreacted state of the TEP in

Table 7
XPS results (Binding Energies, Element/Cation relative concentrations) for the samples Gel_(H_3PO_4/TEPI/TEP).

Sample	BEs (eV)				Element relative concentrations (at.%)				Cation relative concentrations (at.%)	
	C1s	O1s	Si2p	P2p	C	O	Si	P	Si	P
Gel_TEP	284.8 288.0	532.3	103.1	134.4	16.8	60.9	19.0	3.2	84.8	15.2
Gel_TEPI	284.8	532.3	103.2	134.4	2.8	70.9	20.0	6.3	75.8	24.2
Gel_H_3PO_4	284.8	532.4	103.3	134.3	1.8	69.5	21.19	7.5	73.9	26.1

Table 8
XPS results (Binding Energies, BE, Element/Cation relative concentrations) and composition obtained by XPS and XRF for the (H_3PO_4/TEPI/TEP)_700.

Sample	BE (eV)				Element relative concentrations (at.%)				Si/P		P_2O_5/SiO_2
	C1s	O1s	Si2p	P2p	C	O	Si	P	XPS	XRF	XRF
TEP_700	284.8	532.4	103.2	134.4 132.5	4.8	61.6	29.8	2.9 0.9	7.84	7.50	0.1411
TEPI_700	284.8	532.3	103.3	134.3	3.5	68.2	21.3	7.0	3.04	4.63	0.2348
H_3PO_4_700	284.8	532.4	103.3	134.3	3.1	67.9	21.4	7.6	2.81	3.97	0.2674

Gel_TEP is also supported by the XPS data. Thus, its highest carbon content (the C1s line profile in Fig. 10a) shows the presence of two chemical bondings, the C—C from the un-reacted TEP and various moieties of carbon atoms bonded oxygen [43], e.g. C—O from TEP and adsorbed surface contaminants. The characteristic Binding Energy (BE) of the P2p photoelectron peak (134.3 eV) in Fig. 10d suggests the chemical binding of P in $(C_2H_5O)_3PO$ (TEP). The one component of the P(2p) region (Fig. 10d) at 134.3 eV could originate from the P═O and O—P—O contributions of the TEP since the two contributions were hardly distinguishable [44,45].

If intensity of the Raman band at 736 cm^{-1} band (Fig. 3a), due to the P—O symmetric stretch [30], seems alike for the Gel_TEP and liquid TEP, its reduced intensity for the Gel_TEPI (Fig. 3b) sample points out partial hydrolysis state of the TEPI as following:

$$P(OC_2H_5)_3 + yH_2O \rightarrow (C_2H_5O)_{3-y}P(OH)_y + yCH_3CH_2OH \quad (3)$$

$$(C_2H_5O)_{3-y}P(OH)_y + (3-y)H_2O \rightarrow H_3PO_3 + (3-y)CH_3CH_2OH \quad (4)$$

Lack of the P═O bonds, Raman band located at 1261 cm^{-1} [7], is identified for the Gel_(TEPI/H_3PO_4) (see Fig. 3b and c).

The two types of Q_0 lines from ^{31}P MAS NMR spectrum of the Gel_H_3PO_4 could be assigned to some isolated structural units resulting from the initial reaction of the precursors. Although no P—O—Si bonds were reported for the gels dried at low temperatures [46], deconvolution of the wide Raman band within 680–1336 cm^{-1} range for the Gel_TEPI and Gel_H_3PO_4 materials reveals a component at 1150 and 1140 cm^{-1}, respectively (Table 3). The P—O—Si bonds could be obtained by condensation of the non-fully hydrated molecules from reactions (1) and (3) as following:

$$(C_2H_5O)_{4-x}Si(OH)_x + (HO)_yOP(C_2H_5O)_{3-y} \rightarrow (C_2H_5O)_{3-y}(OH)_{y-1}OP-O-Si(OH)_{x-1}(C_2H_5O)_{4-x} + H_2O \rightarrow SiO_2 - P_2O_5 \quad (5)$$

The relative content of the phosphorous (at.%) derived from the P2p photoelectron peak in the gels (Table 7) increases in succession: Gel_TEP (3.2) < Gel_TEPI (6.3) < Gel_H_3PO_4 (7.5). This behavior could be correlated with the phosphorous state in the composition of the gel. It is well known that H_3PO_4 intensively reacts with the TEOS leading to the formation of Si—O—P bondings.

$$Si(OC_2H_5)_3(OH) + H_3PO_4 \rightarrow Si(OC_2H_5)_3 - O - P - O(OH)_2 + H_2O \quad (6)$$

For instance, broader component (FWHM of 1.37 ppm) at −9.64 ppm in the ^{31}P MAS NMR for the Gel_H_3PO_4 (Table 6) in comparison to the Gel_TEPI ((FWHM of 1.07 ppm) might correspond to the condensed P—O—Si species in $O{=}P(OH)_2(OP/OSi)$ [12].

Upshifting by 5–8 cm^{-1} of the stretching modes OC—H, C—H and C—H at the high frequency Raman spectrum of the Gel_TEP in comparison to the TEP (Fig. 5) could be explain by TEP physisorption [47] on the surface of the condensation products of the TEOS.

Structural modifications induced by heat treatment of the gels

Annealing of the Gel_(TEP/TEPI/H_3PO_4) materials at 700 °C, gave phosphosilicate glasses with low content of the organic decomposition and combustion byproducts like graphitic materials (the D and G bands of the sp^2 carbon [35]), as depictable from the Raman spectra in Fig. 3. The glassy nature of the (TEP/TEPI/H_3PO_4)_(700/1000) is supported by the wide Raman bands bellow 700 cm^{-1} due to the *m*-membered rings of the interconnected tetrahedral units, Q_n, of the silicate network and the boson peak around 100 cm^{-1}. Narrower Raman bands in the *first region* of the (TEPI/H_3PO_4)_700 indicate that the two samples are in their intermediate stage of transformation gel-to-glass, i.e. coalescence of the particles in the mesoporous glassy state [28], while the silicate network of the TEP_700 is closer to the one in TEP_1000 glass despite the higher Q_4 condensed silicon units for the Gel_(TEPI/H_3PO_4). The NMR data for the (H_3PO_4/TEPI/TEP)_1000 samples reveal a glassy structure formed mainly of Q_4 fully condensed silicon units and Q_3 condensed phosphorous units. Less interconnected network is observed for the TEP based glass containing also 29% Q_3 silicon units and 1.2% Q_1 phosphorous units (see Tables 4 and 5). Besides the Si—O—Si interconnected Q_4 units and P—O—P interconnected Q_3 units, Si—O—P interconnected Q_4 and Q_3 units are identified in the (H_3PO_4/TEPI/TEP)_1000 glasses, the highest fraction of such interconnected silica and phosphate units being observed for the H_3PO_4 based glass. This is in accordance with literature data [8] on decreasing of the proton conductivity as a consequence of crystalline phase formation in the TEP-derived gels heat treated at 600 °C in comparison to the H_3PO_4-derived materials.

Presence of the 1325 cm^{-1} bands in the TEP_700 and TEP_1000 (Figs. 3 and 4, and Table 2) points out formation of the P═O bondings, typically located at 1390 cm^{-1} in phosphate glasses [2,33]. Despite the unreacted state of the TEP component in the corresponding gel, the peak around 1140 cm^{-1} for the same annealed TEP_700 and TEP_1000 materials in Fig. 3 is an indication of the Si—O—P linkages [2], very likely formed by reaction of the oxidative degradation products of the TEP (corresponding to the second degradation stage with the largest loss in Table 2) with the silica matrix. Given the boiling point of 215 °C and unreacted TEP in the Gel_TEP sample, TEP degradation takes place by two competing processes: oxidation and vaporization. Partial vaporization of TEP is also supported by the smallest P_2O_5/SiO_2 (XRF derived ratio in Table 8) among the (TEP/TEPI/H_3PO_4)_700 samples. However, the pathway and intermediates of the TEP oxidation is controversial. Chernick et al. [48] showed that oxidative degradation of TEP took place as following:

$$OP(OC_2H_5)_3 + 9O_2 \rightarrow OP(OH)_3 + 6CO_2 + 6H_2O \quad (7)$$

Otherwise, Zieger and Fisher [49] reported diethyl phosphate, $P(O)(OH)(OC_2H_5)_2$, monoethyl phosphate, $P(O)(OH)_2(OC_2H_5)$ and orthophosphoric acid, $OP(OH)_3$, as TEP pyrolysis products. The same mechanism of pyrolysis was pointed out by Glaude et al. [50]. Due to the flame retardant ability of TEP, latest TEP degradation mechanism [51] consisted in acidic intermediates as phosphate which could catalyze polymer decomposition to char. This behavior, i.e. different phosphorous intermediates of degradation, along with partial vaporization of TEP, might have explained the better completion of the *m*-membered ring structure of the silicate matrix of TEP_700 in comparison to the (TEPI/H_3PO_4)_700 (Raman band within 130–690 cm^{-1} in Fig. 3).

The A_{1325}/A_{800} ratio of the Raman spectra for the TEP_1000 glass (Table 4) points out its lowest P_2O_5 content among the (TEP/TEPI/H_3PO_4)_1000 glasses, e.g. TEP_1000(1.33) < TEPI_1000(1.55) < H_3PO_4_1000 (2.58). By comparing the TEP derived glass thermally treated at 700 and 1000 °C (Fig. 3), a smaller A_{1325}/A_{800} ratio of 0.73 is calculated for the TEP_700 glass due to its organic residue contamination which gives fluorescent background (removed from the corresponding spectra in Fig. 3) and modification of the intensity of the Raman bands. However, a 1.89 times higher P_2O_5/SiO_2 ratio (Table 8), calculated from the XRF composition data, is found for the H_3PO_4_700 in comparison to the TEP_700, similar to the Raman findings where the H_3PO_4_1000 sample has a 1.94 times higher P_2O_5 content than the TEP_1000. The lowest P_2O_5 content of the thermally treated Gel_TEP supports the TG data on the highest mass loss due to the oxidative decomposition of the TEP during the second stage of the thermal treatment in air.

The cation relative concentrations of the Si and P are rather similar for the Gel_(TEPI/H_3PO_4) materials and their corresponding (TEPI/H_3PO_4)_700 (see XPS data in Tables 7 and 8) data, while

the tendency of Si enriching on the surface, due to elimination of TEP, in the sample TEP_700 is even more pronounced compared to Gel_TEP sample. Among the (TEP/TEPI/H_3PO_4)_700 glasses, the P2p spectrum of the TEP_700 exhibits a different chemistry of the phosphorus with two chemical states (Fig. 11). Analogous to the mixture of the P=O and O—P—O linkages in TEP pointed out before for the Gel_TEP, the P2p component at 134.4 eV might be attributable to the P_2O_5. The presence of P—O—Si linkages in the silicate matrix could trigger a shift of the P2p components to 132.5 eV [44]. Also, surface adsorbed chemical species (e.g. OH groups) could lead to such a peculiar behavior by formation of O—P—OH.

The influence of the different phosphorous precursors studied in the present work on the composition and structure of the resulted gels and glasses could be useful in clearing up the structural and compositional findings as well as optical and electrical properties of the corresponding films previously reported [52,24]. Thus, Vasiliu et al. [52,24] have determined by XPS the complete elimination of P both in the gel state and thermally treated films up to 200 °C (at least at the surface of the films) when TEP was used as reagent. Heat treatment close to the boiling point (215 °C) of the TEP which was physisorptioned, as found here by Raman spectroscopy, in the TEP based films could be the plausible explanation of the phosphorous lack on the surface of these films. Conversely, the presence of the P was noticed in all films prepared with H_3PO_4.

Conclusions

Combining various spectroscopic techniques, i.e. ^{29}Si and ^{31}P MAS NMR, XPS, XRF and Raman, with thermal analysis (TGA) and systematic deconvolution of the spectral data enable us to infer quantitative and qualitative information on the structural modifications underwent by the liquid precursors and the three gels with $90SiO_2$–$10P_2O_5$ composition (named Gel_(TEP/TEPI/H_3PO_4) according to the different phosphorous precursors after heat treatment at 700 and 1000 °C.

In the case of the gel obtained starting with TEP, all methods employed here have established its presence in its unreacted state and less connective silica network among the three gels. By thermal treatment, a competition between TEP evaporation from the corresponding gel and reaction of the TEP degradation products with the silica matrix occurred. Under these circumstances a glass with low amount of Si—O—P bondings is obtained. Conversely, H_3PO_4 reacts with the silica precursor during the sol–gel process and as a result the amount of Si—O—P bondings is the highest. In fact, the presence of the Si—O—P bondings was evidenced by spectral deconvolution even in the gel phase of the phosphosilicate materials with TEPI and H_3PO_4 precursors.

Partial phosphorous depletion for the TEP based glasses in comparison to the predicted $90SiO_2$–$10P_2O_5$ glass is due to the lack of the TEP hydrolysis during the sol–gel process followed by its partial vaporization and oxidative degradation of the physisorptioned TEP to the most likely H_3PO_4 which reacts subsequently with the already formed silica matrix.

Acknowledgements

This paper was carried out within the research program "Materials Science and Advanced Methods for Characterization" of the "Ilie Murgulescu" Institute of Physical Chemistry, financed by the Romanian Academy. Support of the EU (ERDF) and Romanian Government, that allowed for acquisition of the research infrastructure under POS-CCE O 2.2.1 project INFRANANOCHEM – No. 19/01.03.2009, is gratefully acknowledged.

References

[1] G. Lusvardi, D. Zaffe, L. Menabue, C. Bertoldi, G. Malavasi, U. Consolo, Acta Biomater. 5 (2009) 419–428, http://dx.doi.org/10.1016/j.actbio.2008.07.007.
[2] R.E. Noons, R. Devonshire, T.V. Clapp, S.M. Ojha, O. McCarthy, J. Non-Cryst. Solids 354 (2008) 3059–3071, http://dx.doi.org/10.1016/j.jnoncrysol.2007.12.016.
[3] H. Li, X. Chen, F. Jiang, M. Ai, Z. Di, J. Gu, J. Power Sources 199 (2012) 61–67, http://dx.doi.org/10.1016/j.jpowsour.2011.10.032.
[4] C.J. Brinker, G.W. Scherer, Sol–Gel Science, The Physics and Chemistry of Sol–Gel Processing, Academic Press Inc, 1990.
[5] J. Livage, C. Sanchez, J. Non-Cryst. Solids 145 (1992) 11–19, http://dx.doi.org/10.1016/S0022-3093(05)80422-3.
[6] C. Fernanado-Lorenzo, L. Esquivias, P. Barboux, J. Maquet, F. Taulelle, J. Non-Cryst. Solids 176 (1994) 189–199, http://dx.doi.org/10.1016/0022-3093(94)90077-9.
[7] J.-C. Schrotter, A. Cardenas, M. Smaihi, N. Hovnanian, J. Sol–Gel Sci. Technol. 4 (1995) 195–204, http://dx.doi.org/10.1007/BF00488374.
[8] A. Matsuda, T. Kanzaki, Y. Kotani, M. Tatsumisago, T. Minami, Solid State Ionics 139 (2001) 113–119, http://dx.doi.org/10.1016/S0167-2738(00)00819-5.
[9] S.-P. Tung, B.-J. Hwang, J. Membr. Sci. 241 (2004) 315–323, http://dx.doi.org/10.1016/j.memsci.2004.06.003.
[10] S.-P. Szu, L.C. Klein, M. Greenblatt, J. Non-Cryst. Solids 143 (1992) 21–30, http://dx.doi.org/10.1016/S0022-3093(05)80548-4.
[11] N.J. Clayden, S. Esposito, P. Pernice, A. Aronne, J. Mater. Chem. 11 (2001) 936–943, http://dx.doi.org/10.1039/B004107F.
[12] C. Coelho, T. Azais, L. Bonhomme-Coury, J. Maquet, D. Massiot, C. Bonhomme, J. Magn. Reson. 179 (2006) 114–119, http://dx.doi.org/10.1016/j.jmr.2005.11.015.
[13] C. Coelho, F. Babonneau, T. Azaıs, L. Bonhomme-Coury, J. Maquet, G. Laurent, C. Bonhomme, J. Sol–Gel Sci. Technol. 40 (2006) 181–189, http://dx.doi.org/10.1007/s10971-006-7431-x.
[14] H. Aguiar, J. Serra, P. Gonzalez, B. Leon, J. Am. Ceram. Soc. 93 (2010) 2286–2291, http://dx.doi.org/10.1111/j.1551-2916.2010.03733.x.
[15] B.A. Sava, M. Elisa, I.C. Vasiliu, F. Nastase, S. Simon, J. Non-Cyst. Solids 358 (2012) 2877–2885, http://dx.doi.org/10.1016/j.jnoncryso1.2012.07.016.
[16] G. Schottner, Chem. Mater. 13 (2001) 3422–3435, http://dx.doi.org/10.1021/cm011060m.
[17] A. Depla, D. Lesthaeghe, T.S. van Erp, A. Aerts, K. Houthoofd, F. Fan, C. Li, V. Van Speybroeck, M. Waroquier, C.E.A. Kirschhock, J.A. Martens, J. Phys. Chem. C 115 (2011) 3562–3571, http://dx.doi.org/10.1021/jp109901v.
[18] P. Dean, Nature 210 (1966) 257–259, http://dx.doi.org/10.1038/210257a0.
[19] G. Le Saout, P. Simon, F. Fayon, A. Blin, Y. Vaills, J. Raman Spectrosc. 33 (2002) 740–746, http://dx.doi.org/10.1002/jrs.911.
[20] M. Zaharescu, L. Predoana, M. Gartner, M. Anastasescu, L. Todan, P. Osiceanu, C. Vasiliu, C. Grigorescu, G. Pavelescu, Ceram. Eng. Sci. Proc. 28 (2008) 95–106.
[21] M. Zaharescu, A. Vasilescu, V. Bădescu, M. Radu, J. Sol–Gel Sci. Technol. 8 (1997) 59–63, http://dx.doi.org/10.1023/A:1026438820378.
[22] L. Todan, C. Andronescu, D.M. Vuluga, D.C. Culita, M. Zaharescu, J. Therm. Anal. Calorim. 114 (2013) 91–99, http://dx.doi.org/10.1007/s10973-012-2875-4.
[23] M. Anastasescu, M. Gartner, A. Ghiță, L. Predoană, L. Todan, M. Zaharescu, C. Vasiliu, C. Grigorescu, C. Negrilă, J. Sol–Gel Sci. Technol. 40 (2006) 325–333, http://dx.doi.org/10.1007/s10971-006-8775-y.
[24] C. Vasiliu, C. Grigorescu, G. Pavelescu, L. Predoana, L. Todan, M. Gartner, A. Anastasescu, C. Negrila, C. Logofatu, A. Moldovan, M. Zaharescu, J. Optoelectron. Adv. M 9 (2007) 1407–1410.
[25] D. Massiot, F. Fayon, M. Kapron, I. King, S. Le Calve, B. Alonso, J.-O. Durand, B. Bujoli, Z. Gan, G. Hoatson, Magn. Reson. Chem. 40 (2002) 70–76, http://dx.doi.org/10.1002/mrc.984.
[26] A.R. Paschoal, A.P. Ayala, R.C.F. Pinto, C.W.A. Paschoal, A.A. Tanaka, J.S. Boaventura Filho, N.M. Jose, J. Raman Spectrosc. 42 (2011) 1601–1605, http://dx.doi.org/10.1002/jrs.2908.
[27] M. Gnyba, M. Jędrzejewska-Szczerska, M. Keränen, J. Suhonen, Sol–Gel materials investigation by means of Raman spectroscopy, in: Proc. XVII IMEKO World Congress, Dubrovnik, 2003, pp. 237–240.
[28] Ph Colomban, J. Raman Spectrosc. 27 (1996) 747–758, http://dx.doi.org/10.1002/(SICI)1097-4555(199610)27:10<747::AID-JRS38>3.0.CO;2-E.
[29] H. Nakagawa, M. Ochida, Y. Domi, T. Doi, S. Tsubouchi, T. Yamanaka, T. Abe, Z. Ogumi, J. Power Sources 212 (2012) 148–153, http://dx.doi.org/10.1016/j.jpowsour.2012.04.013.
[30] K. Taga, N. Hirabayashi, T. Yoshida, H. Okabayashi, J. Mol. Struct. 212 (1989) 157–168, http://dx.doi.org/10.1016/0022-2860(89)85076-8.
[31] W.W. Rudolph, J. Solution. Chem. 41 (2012) 630–645, http://dx.doi.org/10.1007/s10953-012-9825-4.
[32] B. Kolesov, Am. Mineral. 91 (2006) 1355–1362, http://dx.doi.org/10.2138/am.2006.2179.
[33] A. Saissy, J. Botineau, A. Azema, F. Gires, J. Phys. Lett. 40 (1979) 355–358, http://dx.doi.org/10.1051/jphyslet:019790040014035500.
[34] D.D. Goller, R.T. Phillips, I.G. Sayce, J. Non-Cyst. Solids 355 (2009) 1747–1754, http://dx.doi.org/10.1016/j.jnoncrysol.2009.06.018.
[35] A.C. Ferrari, D.M. Basko, Nat. Nanotechnol. 8 (2013) 235–246, http://dx.doi.org/10.1038/nnano.2013.46.
[36] H. Aguiar, J. Serra, P. Gonzalez, B. Leon, J. Non-Cryst. Solids 355 (2009) 475–480, http://dx.doi.org/10.1016/j.jnoncrysol.2009.01.010.

[37] P. Zhang, C. Dunlap, P. Florian, P.J. Grandinetti, I. Farnan, J.F. Stebbins, J. Non-Cryst. Solids 204 (1996) 294–300, http://dx.doi.org/10.1016/S0022-3093(96)00601-1.
[38] P. Zhang, P.J. Grandinetti, J.F. Stebbins, J. Phys. Chem. B 101 (1997) 4004–4008, http://dx.doi.org/10.1021/jp9700342.
[39] G. Engelhardt, D. Michel, High-resolution Solid State NMR of Silicates and Zeolites, John Wiley, Chichester, 1987.
[40] R.K. Brow, J. Non-Cryst. Solids 263 (2000) 1–28, http://dx.doi.org/10.1016/S0022-3093(99)00620-1.
[41] F. Fayon, D. Massiot, K. Suzuya, D.L. Price, J. Non-Cryst. Solids 238 (2001) 88–94, http://dx.doi.org/10.1016/S0022-3093(01)00357-X.
[42] R. Dupree, D. Holland, M.G. Mortuza, J.A. Collins, M.W.G. Lockyer, J. Non-Cryst. Solids 106 (1988) 403–407, http://dx.doi.org/10.1016/0022-3093(88)90298-0.
[43] G. Beamson, D. Briggs, High Resolution XPS of Organic Polymers. The Scienta ESCA A300 Database, Wiley, Chichester, 1992.
[44] Ph Massiot, M.A. Centeno, M. Gouriou, M.I. Domínguez, J.A. Odriozola, J. Mater. Chem. 13 (2003) 67–74, http://dx.doi.org/10.1039/B208698K.
[45] E.E. Khawaja, S.M.A. Durrani, F.F. Al-Adel, M.A. Salim, M.S. Hussain, J. Mater. Sci. 30 (1995) 225–234. doi: 0022-2461/95.
[46] Ph Massiot, M.A. Centeno, I. Carrizosa, J.A. Carrizosa, J. Non-Cryst. Solids 292 (2001) 158–166, http://dx.doi.org/10.1016/S0022-3093(01)00854-7.
[47] I. Bhowmick, N. Singh, Analyst 139 (2014) 4154–4168, http://dx.doi.org/10.1039/C4AN00629A.
[48] C.L. Chernick, H.A. Skinner, C.T. Mortimer, J. Chem. Soc. (1955) 3936–3938, http://dxdoi.org/10.1039/JR9550003936.
[49] E.J.P. Zeger, E.M. Fisher, Combust. Sci. Technol. 138 (1998) 85–103, http://dx.doi.org/10.1080/00102209808952064.
[50] P.A. Glaude, H.J. Curran, W.J. Pitz, C.K. Westbrook, Proc. Combust. Institute 28 (2000) 1749–1756.
[51] S. Gaan, P. Rupper, V. Salimova, M. Heuberger, S. Rabe, F. Vogel, Polym. Degrad. Stabil. 94 (2009) 1125–1134, http://dx.doi.org/10.1016/j.polymdegradstab.2009.03.017.
[52] C. Vasiliu, M. Gartner, M. Anastasescu, L. Todan, L. Predoană, M. Elisa, C. Negrilă, F. Ungureanu, C. Logofătul, A. Moldovan, R. Bîrjega, M. Zaharescu, Thin Solid Films 515 (2007) 6601–6605, http://dx.doi.org/10.1016/j.tsf.2006.11.106.